ACS Catalysis

Research Article

pubs.acs.org/acscatalysis

Evidence for Metal–Support Interactions in Au Modified TiO_x/SBA-15 Materials Prepared by Photodeposition

Bastian Mei,[†,∥,⊥] Christian Wiktor,[‡,§,∥] Stuart Turner,[§] Anna Pougin,[†] Gustaaf van Tendeloo,[§] Roland A. Fischer,[‡] Martin Muhler,[†] and Jennifer Strunk*[,†]

[†]Department of Chemistry and Biochemistry, Laboratory of Industrial Chemistry, Ruhr-University Bochum, Universitätsstrasse 150, 44780 Bochum, Germany

[‡]Department of Chemistry and Biochemistry, Inorganic Chemistry II, Ruhr-University Bochum, Universitätsstrasse 150, 44780 Bochum, Germany

[§]Electron Microscopy for Materials Science (EMAT), Antwerp University, Groenenborgerlaan, 171, 2020 Antwerpen, Belgium

Supporting Information

ABSTRACT: Gold nanoparticles have been efficiently photodeposited onto titanate-loaded SBA-15 (Ti(x)/SBA-15) with different titania coordination. Transmission electron microscopy shows that relatively large Au nanoparticles are photodeposited on the outer surface of the Ti(x)/SBA-15 materials and that TiO_x tends to form agglomerates in close proximity to the Au nanoparticles, often forming core–shell Au/TiO_x structures. This behavior resembles typical processes observed due to strong-metal support interactions. In the presence of gold, the formation of hydrogen on Ti(x)/SBA-15 during the photodeposition process and the performance in the hydroxylation of terephthalic acid is greatly enhanced. The activity of the Au/Ti(x)/SBA-15 materials is found to depend on the TiO_x loading, increasing with a larger amount of initially isolated TiO_4 tetrahedra. Samples with initially clustered TiO_x species show lower photocatalytic activities. When isolated zinc oxide (ZnO_x) species are present on Ti(x)/SBA-15, gold nanoparticles are smaller and well dispersed within the pores. Agglomeration of TiO_x species and the formation of Au/TiO_x structures is negligible. The dispersion of gold and the formation of Au/TiO_x in the SBA-15 matrix seem to depend on the mobility of the TiO_x species. The mobility is determined by the initial degree of agglomeration of TiO_x. Effective hydrogen evolution requires Au/TiO_x core–shell composites as in Au/Ti(x)/SBA-15, whereas hydroxylation of terephthalic acid can also be performed with Au/ZnO_x/TiO_x/SBA-15 materials. However, isolated TiO_x species have to be grafted onto the support prior to the zinc oxide species, providing strong evidence for the necessity of Ti–O–Si bridges for high photocatalytic activity in terephthalic acid hydroxylation.

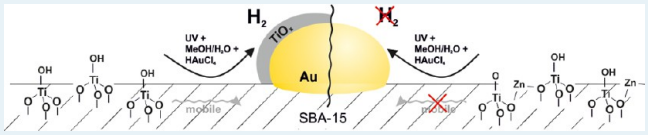

KEYWORDS: *photocatalysis, titanate-loaded SBA-15, Au cocatalysts, strong metal–support interactions, advanced TEM*

INTRODUCTION

Over the past decades, highly dispersed gold nanoparticles on metal oxides have attracted interest as catalysts for several reactions like CO oxidation, selective oxidation of alcohols, or methanol synthesis.[1,2] Recently, the potential of Au nanoparticles in photocatalysis has received considerable attention.[3−7] Several studies have reported improved photocatalytic performance due to the visible light absorption of the Au plasmon and the electron storage capacities of Au.[3,4,8] In general, metal cocatalysts are assumed to act as an electron or hole sink enhancing the electron–hole lifetime in photocatalysis.[3,4] One of the most studied composites in this regard are Au/TiO_2 materials which exhibit catalytic activity in organic pollutant degradation and hydrogen evolution based on photocatalytic reforming of alcohols. The utilized composites are obtained by deposition–precipitation, colloidal synthesis, or photodeposition of Au nanoparticles.[2,4,9−11]

The occurrence of strong metal–support interactions (SMSIs) between oxide supports and noble metal particles upon reduction is usually characterized by H_2 or CO chemisorptions experiments.[12−15] In addition, the characterization of metal–support interactions by advanced electron microscopy is also feasible.[14,16] In the case of TiO_2-supported nanoparticles, it is generally accepted that a thin layer of TiO_x suboxide species covers the metal nanoparticles upon reduction.[13,14,17−19] Recently, Tanaka et al.[20] observed a similar phenomenon for Pt/TiO_2 and Rh/TiO_2 composite materials prepared by photodeposition. For Au/TiO_2 materials prepared by a similar procedure, a weaker interaction between the metal and the support was proposed. However, a partial encapsulation was observed for all metals by XPS depth profiling.[20]

Apart from the versatile materials bulk TiO_2 and Au/TiO_2,[17,21] single-site titania catalysts are widely studied,[22] and find particular use in photocatalytic CO_2 reduction.[23,24] Mori et al.[10,11] showed that the deposition of Au nanoparticles using photoexcited Ti-containing zeolites is feasible. We demonstrated that Au/Ti(x)/SBA composite materials prepared by

Received: October 24, 2013
Published: November 5, 2013

photodeposition of Au were highly active in photocatalytic CO_2 reduction, presumably due to a higher hydrogenation activity of the composite material in the presence of Au nanoparticles.[24] However, the UV−vis spectroscopic results and the XPS characterization showed that the Ti coordination of the isolated TiO_4 tetrahedra changed upon Au photodeposition. Two different TiO_x species were observed by XPS, and UV−vis spectroscopy results indicated that changes in the TiO_x coordination due to the interaction with adsorbed water are less pronounced for the Au/Ti(x)/SBA-15 material.[25] However, the interaction between the TiO_x species and photodeposited Au is still unclear, and the effect of Au on the photocatalytic activity of the Au/Ti(x)/SBA-15 material is not yet clearly identified.

It is known that high loadings of isolated or slightly agglomerated TiO_x species can be obtained reproducibly by grafting $Ti(O^iPr)_4$.[26] The first to show that isolated titania sites are able to perform CO_2 reduction were Anpo et al.[27] Other than for semiconductors the photocatalytic properties arise from a ligand to metal charge transfer (LMCT) where an electron is transferred from an oxygen to a titania atom as a HOMO−LUMO excitation. For the Ti−O−Si bond in isolated titania species, this excitation was estimated to be in the middle UV region depending on the degree of agglomeration of the titania species.[28] In adsorption studies by Stair et al., it was found that these titania species are poor CO_2 adsorbents.[29] In an attempt to improve the adsorption capacities of the material, we were able to introduce ZnO_x species into the materials by grafting of $Zn(acac)_2$.[26] Crucial properties of the photocatalysts such as light absorption, CO_2 adsorption, and basic and acidic sites on the surface of the different materials were studied.[26] It was shown that ZnO_x species significantly enhance the CO_2 adsorption properties, whereas light absorption mainly depends on the HOMO−LUMO excitation of the TiO_x species. XPS and EXAFS showed that Ti−O−Zn bonds are preferably formed when ZnO_x is grafted first.[26] Thus, the coordination of TiO_x can be easily changed using different titania loading or grafting of additional ZnO_x species.

In this contribution, photodeposition of Au nanoparticles on TiO_x- and ZnO_x-grafted SBA-15 has been systematically studied using differently coordinated titania to investigate the interaction of Au and TiO_x species. On the basis of the hydrogen evolution reaction through photoreforming of methanol and the hydroxylation of terephthalic acid, both the electron and the hole availability upon photoexcitation were assessed and the dependence of the photocatalytic activity on the initial titania loading and the presence of ZnO_x species was investigated. By means of transmission electron microscopy, it is shown that Au/TiO_x agglomerates are formed in the absence of ZnO_x. In Ti(x)/SBA-15 samples, the final size of Au particles and their encapsulation by TiO_x species occurring during the diffusion-controlled photodeposition of Au resembles the phenomena of strong-metal support interactions. The encapsulation of Au nanoparticles is slightly affected by the initial TiO_x loading. However, in the presence of ZnO_x, monodisperse Au particles matching the size of the SBA-15 channels are photodeposited homogeneously throughout the whole material, the agglomeration of TiO_x is clearly inhibited, and the formation of TiO_x shells surrounding the Au particles does not occur. Furthermore, our results provide evidence that Ti−O−Si bonds are essential for the photocatalytic activity in the hydroxylation reaction of terephthalic acid.

EXPERIMENTAL SECTION

Sample Synthesis. The synthesis of SBA-15 and the grafting procedure for obtaining isolated and slightly agglomerated TiO_x and ZnO_x species on the SBA-15 surface have been described in detail elsewhere.[26] In brief, $Ti(O^iPr)_4$ (99.999%, Sigma-Aldrich) or $Zn(acac)_2$ (98%, Alfa Aesar, purified by means of sublimation) were dissolved in dry toluene and contacted with the dried SBA-15 support at room temperature. After 4 h of stirring, the solution was removed by sedimentation or centrifugation. Samples were washed three times with dry toluene, dried in vacuum, and calcined. Coverages up to 1 Ti nm^{-2} or 1 Zn nm^{-2} were obtained in a single grafting step, while for higher coverage the grafting procedure had to be repeated. The samples were named according to the transition metal loading obtained by inductively coupled plasma optical emission spectroscopy (ICP-OES); i.e., the sample with a titanium loading of 1.0 Ti nm^{-2} is labeled to Ti1.0/SBA.[26] An overview of the different synthesis steps is given in Figure S1 (Supporting Information).

Characterization. Characterization of the Ti(x)/SBA and the Au-modified materials was performed by elemental analysis, UV−vis spectroscopy, and (scanning) transmission electron microscopy ((S)TEM). In-depth characterization of the different as-received TiO_x- and ZnO_x-grafted SBA-15 supports by means of elemental analysis, nitrogen physisorption, UV−vis spectroscopy, X-ray photoelectron spectroscopy (XPS), and X-ray absorption spectroscopy (XAS) is described elsewhere.[25,26] UV−vis diffuse reflectance spectra (DRS) were recorded in a Perkin-Elmer Lambda 650 UV−vis spectrometer equipped with a Praying-Mantis mirror construction using MgO as the 100% reflection reference.

Bright field TEM, high resolution TEM (HRTEM), electron energy-loss spectroscopy (EELS), and energy-filtered TEM (EFTEM) were performed on a Philips CM30 equipped with a Schottky field emission gun and a postcolumn GIF 200 energy filter operated at 300 kV. High-angle annular dark-field scanning transmission electron microscopy (HAADF-STEM), spatially resolved energy-dispersive X-ray spectroscopy (STEM-EDX), and electron tomography were performed on a FEI Tecnai G2 equipped with a Schottky field emission gun operated at 200 kV and a FEI Titan "cubed" microscope equipped with a probe corrector, operated at 300 kV. EDX spectra were recorded on a Philips CM20 operated at 200 kV.

Photocatalytic Measurements. Photodeposition of Au was performed in a continuous flow stirred-tank reactor equipped with a 700 W Hg immersion lamp, cooled by water circulating in a double wall jacket.[24,30] During photodeposition, the concentrations of CO_2, O_2, and H_2 were analyzed with a non-dispersive IR photometer, a paramagnetic, and a thermal conductivity detector (XStream, Emerson Process Management), respectively. A 350 mg portion of catalyst was dispersed in a solution of 550 mL of dest. H_2O, 50 mL of MeOH, and 3.5 mL of a 1.5×10^{-3} molar auric acid solution ($HAuCl_4$ 99.9%, Sigma Aldrich). The reactor was deaerated for 60 min using pure N_2 prior to irradiation. Photodeposition was performed at 30 °C with 50% irradiation power (350 W) for 2.5 h. After successful photodeposition, the materials were filtered and freeze-dried overnight. Terephthalic acid (TA) hydroxylation was performed to determine the amount of OH radicals generated during irradiation. A 150 mg portion of catalyst was ultrasonicated for 5 min in 500 mL of a 0.01 M NaOH solution containing 3 mM TA.[31,32] The suspension was stirred for an

dx.doi.org/10.1021/cs400964k | ACS Catal. 2013, 3, 3041−3049

additional 30 min in the dark before illumination was started by means of a 150 W Xe immersion lamp cooled by water circulating in a double wall jacket. Samples were taken every 15 min and filtered with a Filtropur S. The fluorescence spectra were measured with a double monochromatic fluorescence spectrometer (Fluorolog FL3-22, HORIBAJobin Scientific). The emission wavelength was set to 320 nm, and the characteristic fluorescence at 426 nm was measured which is directly correlated with the generated OH radicals.

RESULTS AND DISCUSSION

Characterization of the Ti(x)/SBA and Zn(x)/Ti(x)/SBA support materials is reported elsewhere.[26] In short, UV−vis, X-ray photoelectron (XPS), and X-ray absorption spectroscopy (XAS) proved that in dry samples tetrahedrally coordinated TiO_4 species were obtained within the SBA-15 up to Ti loadings of 2.1 wt %, i.e., about 0.3 Ti nm^{-2} (Ti0.3/SBA). Upon increasing of the titania loading, the species start to polymerize; however, for Ti loadings up to 7 wt %, corresponding to about 1 Ti nm^{-2} (Ti1.0/SBA), most of the TiO_x species are still isolated. For all materials, a homogeneous titania distribution was obtained as evidenced by XPS.[26] The Ti distribution was additionally proven to be homogeneous for Ti1.0/SBA in BF and EFTEM (Figure S2, Supporting Information).

A wavelength of less than 300 nm is required to excite electrons across the HOMO−LUMO gap in the case of fully isolated TiO_x species.[26] For agglomerated TiO_x at a loading of 2.7 Ti nm^{-2}, the required wavelength shifts to 320 nm. For the TiO_x- and ZnO_x-grafted SBA-15 samples, namely, Ti1.2/Zn0.3/SBA and Zn0.3/Ti1.2/SBA, strong interactions between TiO_x and ZnO_x were detected.[26] The nature of the TiO_x species depends on the order of grafting steps. More isolated TiO_x species were obtained when ZnO_x was grafted subsequent to TiO_x as in Zn0.3/Ti1.2/SBA.[26]

Photocatalytic Activity in the Presence of Au. Au was photodeposited using methanol as a sacrificial agent.[6,24] The maximum amount of deposited Au was evaluated using a stepwise photodeposition procedure, monitoring the amount of H_2 evolved during photodeposition due to photocatalytic methanol reforming online.[30] All measurements confirmed that H_2 evolution only occurs in a dispersion of Ti(x)/SBA-15 samples in auric acid solution under irradiation, whereas H_2 was not detected in the absence of any of the components. For low Au loadings of 0.05 wt % deposited on Ti2.0/SBA, the evolution of hydrogen slowly increases within 60 min of irradiation time (Figure S3, Supporting Information). Afterward, the Au concentration was increased stepwise. During each deposition, interval irradiation was performed for 60 min. The slow increase in hydrogen evolution was observed for Au loadings of up to 0.35 wt %, at which the H_2 evolution stabilizes. The maximum H_2 evolution was observed for a Au content between 0.45 and 0.55 wt % Au for the Ti2.0/SBA material (Figure S3, Supporting Information). The same trend in hydrogen evolution with increasing Au loading was observed for Ti1.0/SBA (not shown). Bowker et al.[6,7] as well as other groups already reported that there is a maximum amount of cocatalyst, which is beneficial for photocatalytic reactions, because too high loadings might block active sites. From a certain loading on, this would overwhelm the otherwise positive effect of the cocatalyst. Therefore, by the stepwise deposition procedure, Au loadings of up to 0.45 wt % were determined to be still beneficial for the two Ti(x)/SBA materials.

In a second set of experiments, the amount of Au in the solution was fixed to 0.25 wt % to study the effect of the different Ti loadings as well as the effect of Zn. A lower amount of Au was chosen to avoid blocking of active sites in samples with a lower TiO_x loading. Furthermore, a loading of 0.25 wt % Au was already shown to enhance the photocatalytic activity for similar materials with low titania loadings.[24] The evolution of H_2 as a function of irradiation time during the in situ photodeposition experiments is shown in Figure 1 for different

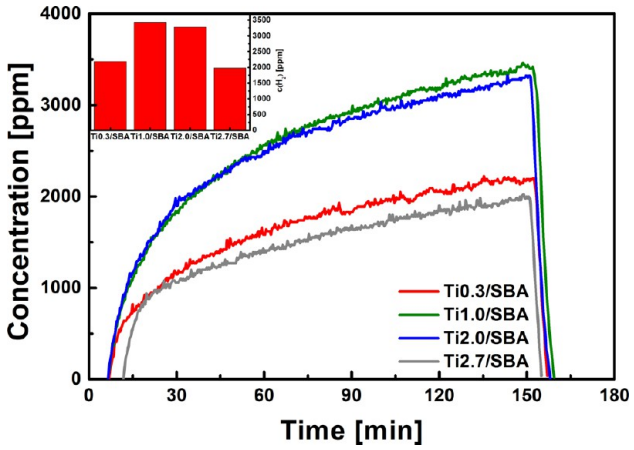

Figure 1. H_2 evolution measured during the photodeposition process of Au (0.25 wt %) on Ti(x)/SBA materials with increasing Ti loading.

Ti(x)/SBA materials. From these results, it can clearly be seen that the detectable amount of H_2 in the gas phase significantly increases with the Ti loading up to 7 wt % as in Ti1.0/SBA, while it decreases at higher Ti loadings as in the case of Ti2.0/SBA and Ti2.7/SBA. This trend is a first indication for different activities of isolated and polymerized TiO_x species. Ti1.0/SBA is more active than Ti0.3/SBA; however, in both cases, the Ti species are mainly isolated and have a tetrahedral coordination sphere in the dry state.[26] Those species should be entirely surrounded by Ti−O−Si bonds and are able to coordinate two water molecules, upon which they change into an octahedral configuration.[33] In the case of the higher loaded Ti1.0/SBA, more of these isolated species can contribute to the H_2 generation. With increasing TiO_x loadings, the evolved H_2 drops off due to polymerization of the TiO_x species because less isolated TiO_4 sites can contribute to the hydrogen generation. The beneficial effect of Au supported on different semiconductors in photocatalytic H_2 production or photocatalytic dye degradation has already been demonstrated by several research groups.[3,4] It is supposed that Au-containing materials show enhanced dye degradation rates and a significant increase in H_2 productivity due to efficient electron storage on the Au nanoparticles, which result in a decrease in recombination rates, and due to the ability of the Au nanoparticles to act as an electron transfer site.[3,8] An influence of the Au loading on the H_2 production rate has been reported recently.[3,6] In the present study, the influence of Au loading on the H_2 evolution rate was confirmed for the Ti(x)/SBA materials. Furthermore, at a fixed Au loading, the obtained results indicate an effect of the TiO_x coordination and agglomeration on the hydrogen evolution ability.

Changes in the titania coordination by the incorporation of ZnO_x species were investigated using Zn0.3/Ti1.2/SBA and Ti1.2/Zn0.3/SBA catalysts. It was recently shown that the

dx.doi.org/10.1021/cs400964k | ACS Catal. 2013, 3, 3041−3049

change in titania coordination is less pronounced for materials in which ZnO_x is grafted subsequently to titania as in Zn0.3/Ti1.2/SBA.[26] Thus, it can be assumed that the amount of Ti−O−Si bonds is less affected for Zn0.3/Ti1.2/SBA. However, for both materials, H_2 evolution was not observed during deposition of 0.25 wt % Au, even though, similar to the Ti(x)/SBA samples, Zn0.3/Ti1.2/SBA and Ti1.2/Zn0.3/SBA became purple/bluish after the experiments, indicating the deposition of Au nanoparticles. Nevertheless, the absence of H_2 evolution clearly points to differences in the properties of Au/Ti(x)/SBA compared to the Zn-containing and Au/Zn0.3/Ti1.2/SBA and Au/Ti1.2/Zn0.3/SBA samples. Furthermore, it should be mentioned that within the detection limit no hydrogen evolution was observed for the Zn0.3/SBA sample or the bare SBA-15 support and the samples remained white after the photodeposition experiments.

Measurements of the photocatalytic H_2 evolution mainly probe the availability of photogenerated electrons upon light irradiation. To probe the availability of photogenerated holes for photocatalytic reactions, hydroxylation of terephthalic acid (TA) was used as a simple test reaction. It is known that TA reacts with OH radicals, which are formed upon reaction of surface adsorbed water or hydroxyl groups, to form 2-hydroxy terephthalic acid (TAOH). In its terephthalate form, TAOH emits unique fluorescence at around 425 nm.[32,34] First, the as-prepared Ti(x)/SBA and TiO_x- and ZnO_x-grafted SBA-15 materials were tested. They did not show significant photocatalytic activity for the hydroxylation of TA under the experimental conditions. Two possible reasons for the low activity are the low intensity of deep UV light and a fast electron−hole recombination. The influence of the latter should be diminished using the Au-modified Ti(x)/SBA and TiO_x- and ZnO_x-grafted SBA-15 samples obtained after photodeposition experiments.

The TA hydroxylation test reaction was repeated with the Au/Ti(x)/SBA, Au/Zn0.3/Ti1.2/SBA, and Au/Ti1.2/Zn0.3/SBA samples. The obtained results are shown in parts a and b of Figure 2, respectively. The TA test results indicate that the Au/Ti(x)/SBA materials are able to generate OH radicals, which can easily react with terephthalic acid to form TAOH, whereas Au/SBA is nearly inactive. Furthermore, the almost linear relationship between irradiation time and fluorescence signal intensity indicates that Au/Ti(x)/SBA-15 materials are stable under these reaction conditions. The small amount of TAOH formed in the case of Au/SBA-15 may be related to surface hydroxyl groups of the SBA-15 support participating in the reaction. In a blank experiment without the addition of a catalyst or the bare SBA-15 substrate material, no reaction was observed.

Among the Au/Ti(x)/SBA materials, Au/Ti1.0/SBA shows the highest production rate of TAOH. The higher loaded samples Au/Ti2.0/SBA and Au/Ti2.7/SBA and the Au/Ti0.3/SBA sample with lower Ti loading are clearly less active. Samples Au/Ti0.3/SBA and Au/Ti1.0/SBA contain many isolated TiO_4 species, as shown by XAS and XPS,[26] while the higher loaded samples contain mainly polymerized TiO_x chains, which appear to be less active. It is striking that the activity of Au/Ti0.3/SBA is as low as the activity of Au/Ti2.7/SBA, even though it was shown that only isolated TiO_x species are present. This observation may be attributed to the larger absorption edge energy in the case of Ti0.3/SBA or the lower amount of active TiO_x centers. However, the observed trend in the TA test reaction is in good agreement with the hydrogen

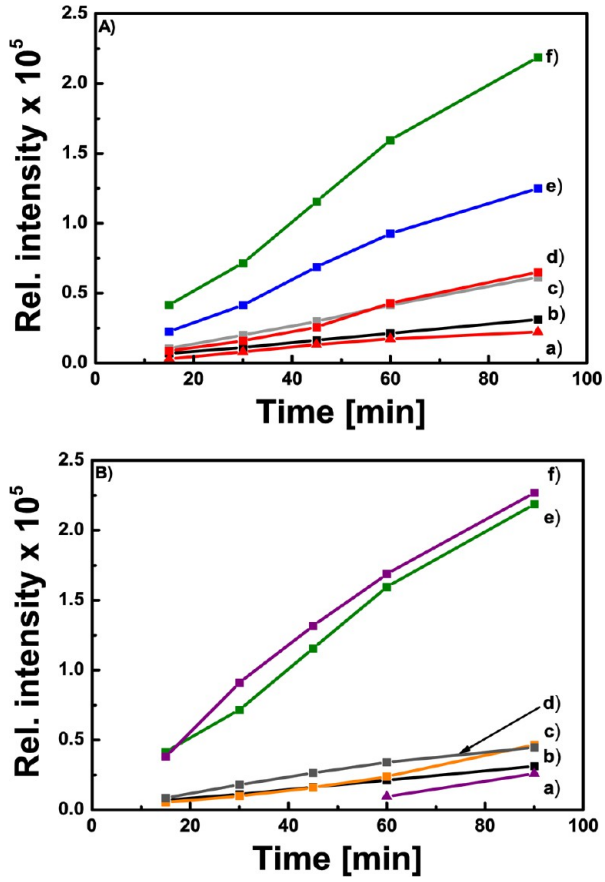

Figure 2. (A) Time-dependent terephthalic acid hydroxylation reaction for (a) Ti0.3/SBA, (b) Au/SBA, (c) Au/Ti2.7/SBA, (d) Au/Ti0.3/SBA, (e) Au/Ti2.0/SBA, and (f) Au/Ti1.0/SBA. (B) Time-dependent terephthalic acid hydroxylation reaction for (a) Zn0.3/Ti1.2/SBA, (b) Au/SBA, (c) Au/Zn0.3/SBA, (d) Au/Ti1.2/Zn0.3/SBA, (e) Au/Ti1.0/SBA, and (f) Au/Zn0.3/Ti1.2/SBA.

evolution rates obtained during Au photodeposition. Thus, the results strongly suggest that isolated TiO_x species are required to achieve high activities in the TA hydroxylation reaction and the photocatalytic reforming of methanol.

The time-dependent evolution of hydroxylated TA for all Zn-containing SBA-15 samples is shown in Figure 2b. Au/Ti1.0/SBA is shown for comparison. While Au/Zn0.3/Ti1.2/SBA is at least as active as Au/Ti1.0/SBA, the other two Zn-containing samples, especially Au/Zn0.3/SBA, are significantly less active in the TA hydroxylation test reaction. These results indicate that TiO_x species rather than ZnO_x species bound to the silica surface are the photocatalytically active species. Furthermore, these results demonstrate that the order of the grafting steps influences the photocatalytic activity: Au/Ti1.2/Zn0.3/SBA is less active than Au/Zn0.3/Ti1.2/SBA. In the case of Au/Ti1.2/Zn0.3/SBA, TiO_x is grafted onto Zn0.3/SBA; thus, it is likely that Ti−O−Zn bonds are formed rather than Ti−O−Si bonds. Indeed, the characterization results based on XPS and XAS indicate an intense interaction between Zn and Ti in samples prepared with a similar composition as the Au/Ti1.2/Zn0.3/SBA material.[26] In the opposite case of Au/Zn0.3/Ti1.2/SBA, where ZnO_x is grafted after TiO_x grafting is completed, the photocatalytic activity in TA hydroxylation is still high. For this material, it can be assumed that Ti−O−Si bonds are formed during the first grafting step and that the formation of Zn−O−Ti bonds due to the post-grafting of ZnO_x is negligible. In

dx.doi.org/10.1021/cs400964k | ACS Catal. 2013, 3, 3041−3049

summary, a structure−activity correlation was observed for the ZnO_x-containing materials, as the order of the grafting steps significantly influences the photocatalytic activity, especially in the TA hydroxylation test reaction. Ti−O−Si bonds rather than Ti−O−Zn bonds are required to run the catalytic reaction. Additionally, it was shown that ZnO_x species are not able to perform the photocatalytic TA hydroxylation reaction, which is in agreement with their poor absorption properties.[26]

Comparison of the photocatalytic activity toward hydroxylation of TA of all the as-prepared and Au-modified samples clearly demonstrates that Au is able to enhance the photocatalytic activity of both Ti(x)/SBA and ZnO_x/TiO_x/SBA samples. Presumably, Au is acting as a cocatalyst in these cases. On the basis of these results, Au may act as an electron sink or it may additionally enable the materials to be activated by visible light due to the Au plasmon absorption. Recent results for photocatalytic CO_2 reduction indicate that visible-light-driven CO_2 reduction by excitation of the Au plasmon was not feasible for the Au/Ti03/SBA catalyst.[24] Thus, Au should mainly act as an electron sink in these samples. However, it is striking that, even in the presence of Au, photocatalytic reforming of methanol was not possible for Au/Zn0.3/Ti1.2/SBA, as no H_2 was evolved. On the other hand, Au/Zn0.3/Ti1.2/SBA exhibited similar photocatalytic activity toward TA hydroxylation as the most active Au/Ti1.0/SBA sample. In order to elucidate this phenomenon, the nature of Au particles in the different materials was characterized by means of ICP-OES, UV−vis spectroscopy, and TEM analysis.

Characterization of the Au Particles. ICP-OES results indicate that the amount of deposited Au for the Au/Ti(x)/SBA materials is in good agreement with the expected loading of 0.25 wt % supplied during the photodeposition procedures (Table S1, Supporting Information). As expected, Au can barely be deposited on Au/SBA, most likely due to a lack of photoactive sites. The small amount of Au found on Au/SBA was probably formed due to a simple decomposition or photobleaching process of auric acid on the support, which is not necessarily photoinduced. For the Zn-containing materials Au/Zn0.3/Ti1.2/SBA and Au/Ti1.2/Zn0.3/SBA, the results clearly indicate that less Au was deposited; however, the results also show that the presence of TiO_x species is required for the photodeposition of Au driven by a photocatalytic reduction of auric acid. In Au/Zn0.3/SBA, only a small amount of Au was detected by ICP-OES, very similar to the amount of Au deposited on the bare SBA-15. In both cases, the deposition of Au may be related to a photobleaching process of auric acid solution instead of a photocatalytic reduction. Additionally, ICP-OES results confirmed that leaching of Ti or Zn species during the photodeposition process can be neglected (results not shown).

The structure and position of the Au plasmon peaks were analyzed by UV−vis spectroscopy (Figure S4a and b, Supporting Information). Except for Au/SBA and Au/Zn0.3/SBA, all materials showed a characteristic Au plasmon absorption signal. There are slight differences in the position of the plasmon absorption depending on the Ti loading and presence of ZnO_x species. In general, a plasmon centered at a wavelength higher than 550 nm is observed for all Au/Ti(x)/SBA samples after photodeposition of 0.25 wt % Au. For the subsequently grafted samples Au/Zn0.3/Ti1.2/SBA and Au/Ti1.2/Zn0.3/SBA, the plasmon peak is also centered at ∼550 nm. It can be assumed that metallic Au is present, since the plasmon of Au in the metallic state is accepted to be in the range 500−600 nm (Figure S4b, Supporting Information).[35,36] From the plasmon maximum position, it can be assumed that the Au nanoparticles are approximately 10 nm in size.[35,37,38] However, there are certain differences in the nature of photodeposited Au nanoparticles in the Zn-containing samples. A more intense Au plasmon was observed in the case of Au/Ti1.2/Zn0.3/SBA, and the overall intensity of the Au plasmon of the Zn-containing samples is lower as compared to the Au/Ti(x)/SBA materials. This is in good agreement with the ICP-OES results, which indicate that less Au was photodeposited. However, the Au/Ti1.2/Zn0.3/SBA sample with a lower loading of Au exhibits a more intense plasmon peak, possibly due to different scattering properties of the material.[35,38]

Advanced TEM analysis was performed for the samples with similar TiO_x loading: Ti1.0/SBA, Au/Ti1.0/SBA, Au/Zn0.3/Ti1.2/SBA, and Au/Ti1.2/Zn0.3/SBA. Bright-field (BF) TEM images show the presence of intact channels, as expected for SBA-15 mesoporous materials (e.g., Figures 3a and 5a for Au/Ti1.0/SBA and Au/Zn0.3/Ti1.2/SBA, respectively). The channels are highly ordered and exhibit a channel spacing with an average distance of ca. 10 nm, determined by Fourier transform (FT) analysis (Figures 3b and 5b).

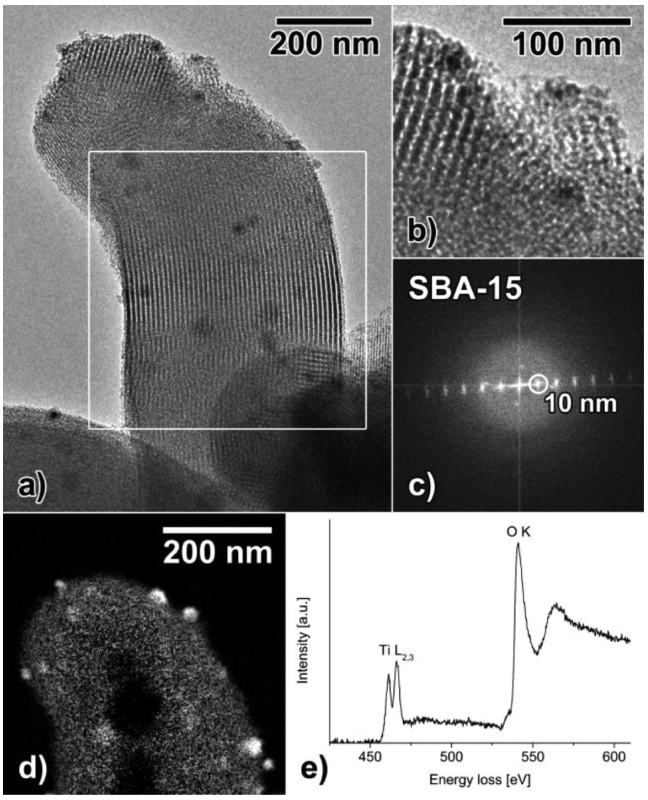

Figure 3. (a) Typical BF-TEM of Au/Ti1.0/SBA. NPs are imaged as dark contrast and are polydisperse. The SBA-15 channels are visibly intact. (b) In higher magnification, the core shell structure of the particles becomes visible. (c) A FT analysis of the white frame in part a shows the pore spacing to be 10 nm. (d) EFTEM Ti map of the tip of the crystal visible in part a. Some of the particles visible in part a give rise to strong Ti signals. Some of the bright Ti enrichments exhibit a slightly darker contrast in their centers, pointing to Ti rich particle shells. Besides the particles, a clear Ti background is present throughout the material. The dark area in the middle of the crystal is due to thickness effects. (e) EELS spectrum of Au/Ti1.0/SBA showing the Ti−$L_{2,3}$ and the O−K edge.

dx.doi.org/10.1021/cs400964k | ACS Catal. 2013, 3, 3041−3049

BF-TEM and energy-filtered (EF) TEM of Ti1.0/SBA show a homogeneous Ti distribution in an otherwise empty framework (Figure S2, Supporting Information). In Au/Ti1.0/SBA, however, contrast features visible in BF-TEM (Figure 3a) indicate the presence of polydisperse nanoparticles with diameters ranging from 10 to 90 nm. At higher magnification, a core−shell structure becomes visible (Figure 3b). A FT analysis of the white frame in part a shows a regular pore spacing of 10 nm. An elemental Ti map was acquired by EFTEM based on the Ti−$L_{2,3}$ edge detected by EELS (Figure 3d and e). The map shows Ti enrichments at positions that coincide with the positions of the particles in the BF-TEM image (Figure 3a). Some measurements show darker areas in the center of the Ti enrichments, i.e., Ti depletion in the center of the particles. Thus, the shells of the particles appear to be rich in Ti but not their cores. Otherwise, the Ti distribution in the Au/Ti1.0/SBA is homogeneous. HR HAADF-STEM (Figure 4) and STEM-EDX (Figure S5, Supporting Information) were used to further explore the nature of these polydisperse core−shell structured particles.

Mass−thickness sensitive HAADF-STEM imaging reveals that the shell of the nanoparticles, and some of the particles themselves, exhibits only a small contrast difference with respect to the framework material (Figure S5a and b, area 2, Supporting Information). This low contrast together with the Ti enrichment detected by EFTEM indicates that the shells consist of TiO_x. The particles were further characterized by high resolution (S)TEM (vide infra).

The cores of the particles in Au/Ti1.0/SBA were indicated to be Au nanoparticles by their stronger image contrast with respect to the framework material and the according STEM-EDX spectrum (Figure S4d, Supporting Information). They were further investigated by FT analysis of the high resolution HAADF-STEM data. Particle A in Figure 4a exhibits multiple twinning defects, typical for small Au nanoparticles. The position and orientation of the defect planes are indicated by white arrows. The FT (Figure 4c) of the HR HAADF-STEM image shows only reflections fitting to the FCC Au crystal structure. Figure 4b shows a typical low-contrast amorphous shell surrounding the gold nanoparticle. Au particle B (Figure 4d) is smaller than A and is imaged along its [111] zone axis, as proven by the FT analysis (Figure 4e). A three-dimensional reconstruction of Au/Ti1.0/SBA by electron tomography revealed that the Au particles are spread throughout the whole framework (Figure S6, Supporting Information). The particles on the outer surface of the crystal seem to be generally larger.

Even though analysis was not performed in the same detail, TEM images of the Au/Ti0.3/SBA and Au/Ti2.0/SBA revealed that polydispersed nanoparticles were formed, as observed for Au/Ti1.0/SBA. Furthermore, it can be assumed that the Au particles detected for Au/Ti0.3/SBA and Au/Ti2.0/SBA are embedded in similar shells (shown for Au/Ti1.0/SBA in Figure 4b). It is likely that the formation of these core−shell structures and the Ti enrichment in the Au/Ti1.0/SBA sample observed at several positions occurs during photodeposition of Au, because the presence of Ti-rich areas was excluded by TEM measurements for the Ti1.0/SBA support sample.

The TEM results presented above and the photocatalytic activity data provide evidence that highly active isolated or slightly polymerized TiO_x were obtained by the anhydrous grafting of $Ti(O^iPr)_4$ on the SBA-15 supports. The isolated species appear to be mobile, at least during photodeposition of

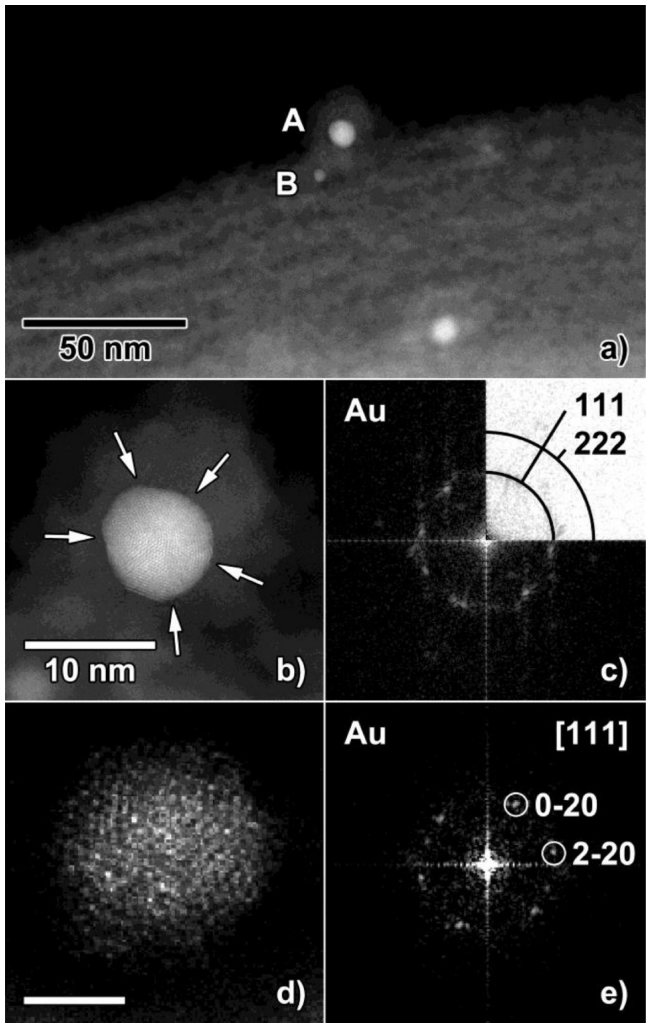

Figure 4. (a) HAADF-STEM image of Au/Ti1.0/SBA showing the presence of several Au nanoparticles (bright white contrast). (b) High-resolution HAADF-STEM image of a single Au nanoparticle A, covered by a low-contrast, amorphous shell. (c) The FT analysis of part b confirms the particle is crystalline Au. (d) Au nanoparticle B imaged along the [111] zone axis orientation, as evidenced by FT analysis shown in part e (scale bar 2 nm).

nanoparticular Au, and tend to agglomerate during the irradiation process. Due to the high photocatalytic activity of the initially isolated and subsequently agglomerated TiO_x species, photodeposition of Au nanoparticles mainly takes place at the outer surface: larger Au particles are photodeposited, and the probability of Au precursor diffusion into the channels of the Au/Ti(x)/SBA samples is low. The photodeposition of larger Au particles embedded in Ti-rich shells was observed for all Au/Ti(x)/SBA samples. A relation between the H_2 evolution activity and these in situ generated Au/TiO_x core shell composites is likely. Even though it was not possible to unequivocally confirm this relationship by means of TEM, the observed trends of photocatalytic hydrogen evolution by methanol reforming for the Au/Ti(x)/SBA samples may be explained as follows: Less H_2 was evolved during Au photodeposition in the presence of Ti0.3/SBA as compared to Ti1.0/SBA, due to the lower TiO_x loading. When increasing the TiO_x loading, as in Ti2.0/SBA or in Ti2.7/SBA, less H_2 was evolved during photodeposition. Ti2.0/SBA and Ti2.7/SBA exhibited less isolated TiO_x species. Instead, TiO_x species are

dx.doi.org/10.1021/cs400964k | ACS Catal. 2013, 3, 3041−3049

present as oligomers and even polymerized TiO_x at the surface of the SBA-15.[26] Presumably, these interconnected TiO_x species are less mobile at the surface and only remaining isolated TiO_x sites are able to move. Thus, less Au/TiO_x core−shell composites can be formed in the photodeposition, resulting in less active sites and lower H_2 evolution. Ti−O−Si bonds may still be needed to be present in the agglomerates formed around the gold nanoparticles, as the composition of the shell was confirmed to be TiO_x enriched, but generally similar to the framework of the material.

The observed behavior of Ti(x)/SBA-15 materials during Au photodeposition resembles the SMSI effect observed for metal/TiO_2 materials. It is widely accepted that upon reduction of metal/TiO_2 materials TiO_x suboxide species ($x < 2$) migrate onto metal particles.[12,14,18,19] It was suggested by Fu et al.[18] that the migration of TiO_x suboxide species ($x < 2$) occurs, when the surface energy of the metal is above 2 J m^{-2} and the metal's work function is larger than the work function of TiO_2. This is particularly the case for Pt, Pd, and Rh metal particles. While a reductive atmosphere is usually necessary to facilitate the migration of the suboxide species, it was recently confirmed by Tanaka et al.[20] that strong metal−support interactions can be observed for metal/TiO_2 composites prepared by photodeposition. Pt, Rh, and Au were photodeposited, and the metal particles were always found to be partially covered by TiO_x suboxides. The observation was explained by the formation of TiO_x species under irradiation and the preferred formation of metal particles at defect sites in the photodeposition process.[20] Indeed, the formation of an amorphous TiO_2 layer containing Ti^{3+} species during irradiation of TiO_2 particles in aqueous solution was recently confirmed by in situ HRTEM.[39] Among the different metals, Au was found to be covered to a lower extent.[20]

The state of titania present in the Ti(x)/SBA-15 materials can be considered as a TiO_x suboxide species. Furthermore, the desired reduction of titania can be achieved by UV-light excitation of the isolated Ti sites. In contrast to TiO_2 particles, the charges are localized and Ti^{3+} sites are generated. Therefore, it can be considered that the migration onto the Au particles is simplified in the case of Ti(x)/SBA-15 materials. The SMSI effect is in good agreement with the considerations of an enhanced mobility of the titania species in Ti(x)/SBA-15.

For Au/Zn0.3/Ti1.2/SBA, the presence of polydispersed core−shell nanoparticles as observed for Au/Ti1.0/SBA was excluded. The Au particles incorporated by photodeposition into the Au/Zn0.3/Ti1.2/SBA sample were hardly visible in BF-TEM (Figure 5a). EFTEM elemental maps based on the Ti−$L_{2,3}$ edge detected by EELS (Figure S7, Supporting Information) show a homogeneous Ti distribution without any enrichment (Figure 5b). HAADF-STEM images show the photodeposited Au particles incorporated in the material (Figure S8, Supporting Information). Some isolated large particles on the outer surface are actually agglomerates of Au particles (Figure 5c). Most of the Au particles are monodispersed, with an average size of 8 ± 2 nm (see size distribution in Figure S9, Supporting Information). A 2D line scan was performed in STEM-EDX to measure the Ti and Zn distribution. Both elements are evenly distributed, as is proven by comparison of the intensity profile with the corresponding element profiles in Figure 5d. Additionally, the presence of Ti, Zn, and Au in Au/Zn0.3/Ti1.2/SBA was proven by EDX acquired in parallel illumination mode (Figure S10, Supporting Information).

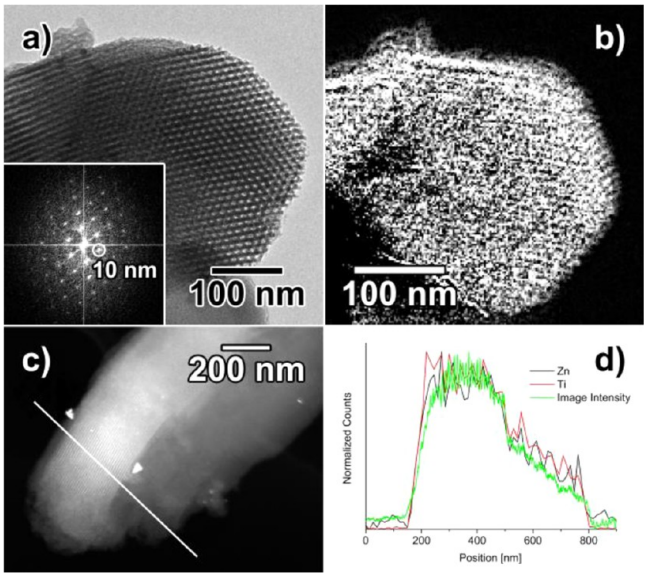

Figure 5. (a) HRTEM image of a typical Au/Zn0.3/Ti1.2/SBA crystal. The channels are visibly intact. Inset: The FT of part a reveals an average distance of 10 nm. (b) EFTEM Ti map of the crystal shown in part a. The Ti distribution is homogeneous. There are no visible Ti enrichments. The dark area on the left side is a thickness effect, and is not due to the absence of Ti. (c) HAADF-STEM image of a typical Au/Zn0.3/Ti1.2/SBA crystal. (d) HAADF-STEM image signal intensity and Ti−K/Zn−L EDX intensity profiles over the white line in part c from the top left to the bottom right (Zn−L, black; Ti−K, red; image intensity, green).

Finally, the position of the Au nanoparticles within the Au/Zn0.3/Ti1.2/SBA material was investigated by electron tomography. Figure S11 (Supporting Information) shows a slice through the three-dimensionally reconstructed volume of the investigated Au/Zn0.3/Ti1.2/SBA material. The intact SBA-15 channels are resolved in the reconstruction, and the Au particles are visibly distributed throughout the Au/Zn0.3/Ti1.2/SBA material. The artifacts in the reconstruction (e.g., elongations of bright spots/Au particles) are a result of the missing wedge and the tendency of the material to charge under the electron beam which can result in movement of the SBA-15 crystal.

TEM measurements unambiguously show that the larger Au particles and Ti-rich areas observed for the Au/Ti1.0/SBA do not exist in the Au/Zn0.3/Ti1.2/SBA sample. The TEM results are supported by UV−vis measurements, which reveal that the intensity of the characteristic Au plasmon (~550 nm) of the Au/Zn0.3/Ti1.2/SBA sample is less intense. Monodispersed homogeneously distributed Au particles within a mesoporous matrix should possess a less intense Au plasmon compared with larger particles mainly situated at the outer surface of a material.[40] However, it needs to be pointed out that the gold loading differs in all samples and that the UV−vis spectra were recorded in diffuse reflectance, so a precise quantitative discussion of the plasmonic effect per particle or per weight of gold is not possible.

Taking this into account, small Au particles mainly in the pores of the material are also expected for the Au/Ti1.2/Zn0.3/SBA sample. This was confirmed by BF-TEM and HAADF-STEM (Figure S12, Supporting Information). However, a slight enrichment of Ti in certain areas possibly associated with larger

dx.doi.org/10.1021/cs400964k | ACS Catal. 2013, 3, 3041−3049

particles was observed in the Ti EFTEM images for Au/Ti1.2/Zn0.3/SBA (Figure S12, Supporting Information).

The photocatalytic activity of the different materials clearly decreases in the order Au/Ti1.0/SBA > Au/Zn0.3/Ti1.2/SBA > Au/Ti1.2/Zn0.3/SBA as Au/Ti1.0/SBA was active for both the evolution of H_2 and the hydroxylation of TA. Regarding the presented TEM characterization results, these differences in photocatalytic activity can be explained by the enrichment in TiO_x and the differences in the particle sizes of the incorporated Au nanoparticles. In the case of Au/Zn0.3/Ti1.2/SBA and Au/Ti1.2/Zn0.3/SBA, monodisperse, evenly distributed particles are photodeposited in the channels and at the outer surface of the material. Furthermore, less Au is deposited on both samples compared to Au/Ti(x)/SBA materials, as evidenced by ICP-OES measurements. The mobility of the TiO_x species after subsequent deposition of ZnO_x appears to be lower or is even inhibited in analogy to the higher loaded Ti2.0/SBA and Ti2.7/SBA samples, and thus, the agglomeration of TiO_x is inhibited. The TiO_x species remain mainly isolated and the photodeposition of Au is slow for the Zn0.3/Ti1.2/SBA sample, resulting in a lower Au loading after 90 min of irradiation. The H_2 evolution by photoreforming of methanol, if occurring at all, is below the detection limit. Nevertheless, the Au/Zn0.3/Ti1.2/SBA and Au/Ti1.0/SBA samples exhibit similar photocatalytic activities toward TA hydroxylation.

In summary, it can be assumed that two different sites are responsible for the hydrogen evolution reaction and the TA hydroxylation, that is, Au/TiO_x agglomerates and Au in close contact to isolated TiO_x species. The Au/TiO_x agglomerates arranged in a core−shell-like structure formed due to strong metal−support interactions, and a high mobility of isolated TiO_x species as observed for Au/Ti(x)/SBA samples may be responsible for the H_2 evolution, whereas Au in close contact to isolated TiO_x species facilitates the hydroxylation of TA. Electron tomography showed that the latter species are present both in Au/Ti1.0/SBA and Au/Zn0.3/Ti1.2/SBA. Consequently, the materials possess similar activities in the hydroxylation of TA. The low activity of Au/Ti1.2/Zn0.3/SBA compared with the activity of Au/Zn0.3/Ti1.2/SBA in TA hydroxylation, although the Au distribution is similar, can be exclusively assigned to the formation of Ti−O−Zn bonds instead of Ti−O−Si bonds.

CONCLUSIONS AND OUTLOOK

Au/Ti(x)/SBA-15 samples are photocatalytically active both in hydrogen production by photoreforming of methanol and in the hydroxylation of terephthalic acid. Therefore, the availability of electrons and holes upon photoexcitation is confirmed. Furthermore, a correlation of titania loading and photocatalytic activity is observed: the highest activity is observed for materials with the majority of initially isolated titania sites. In contrast to the behavior of Au/Ti(x)/SBA, the photocatalytic activity is drastically changed upon incorporation of zinc oxide species as in Au/Zn0.3/Ti1.2/SBA and Au/Ti1.2/Zn0.3/SBA. A photocatalytic activity resembling the activity of the most active Au/Ti(x)/SBA is only observed for Au/Zn0.3/Ti1.2/SBA. The differences in activity are attributed to titania species in a Zn−O−Ti environment, which appeared to be unfavorable for the photocatalytic activity. Moreover, TEM studies indicated a diffusion-controlled photodeposition of Au for Ti(x)/SBA, where larger Au particles are detected at the outer surface. The Au particles in Au/Ti(x)/SBA are mostly associated with a shell of TiO_x species formed due to strong metal−support interactions. These agglomerates are absent or at least less pronounced in Au/Zn0.3/Ti1.2/SBA and Au/Ti1.2/Zn0.3/SBA. Only small Au particles in the channels of SBA-15 are observed. The presence of ZnO_x seems to decrease the mobility of titania species required to form the Au−Ti agglomerates which are the active sites for the H_2 evolution reaction.

ASSOCIATED CONTENT

Supporting Information

Additional TEM and tomography data, diffuse reflectance UV−vis spectra of Au-modified materials, Au content determined by ICP-OES, and H_2 evolution during stepwise photodeposition. This material is available free of charge via the Internet at http://pubs.acs.org.

AUTHOR INFORMATION

Corresponding Author

*E-mail: jennifer.strunk@techem.rub.de. Phone: +49 234 32 23566.

Present Address

[⊥]Technical University of Denmark, Department of Physics, Fysikvej, Building 307, 2800 Kongens Lyngby, Denmark.

Author Contributions

[∥]These authors contributed equally.

Notes

The authors declare no competing financial interest.

ACKNOWLEDGMENTS

This work was funded by the German Ministry of Education and Research (BMBF) within the scope of the funding program "Technologies for Sustainability and Climate Protection − Chemical Processes and Use of CO_2". The authors acknowledge support from the European Union under the Framework 7 program under a contract from an Integrated Infrastructure Initiative (Reference 262348 ESMI). S.T. gratefully acknowledges financial support from the Fund for Scientific Research Flanders (FWO). G.v.T. acknowledges the ERC grant N°246791 − COUNTATOMS and the IAP program of the Belgian government. The Titan microscope used for this work was partially funded by the Hercules Foundation. B.M. acknowledges the Ruhr University Research School for financial support.

REFERENCES

(1) (a) Strunk, J.; Kähler, K.; Xia, X.; Comotti, M.; Schüth, F.; Reinecke, T.; Muhler, M. *Appl. Catal., A* **2009**, *359*, 121−128. (b) Kähler, K.; Holz, M. C.; Rohe, M.; Strunk, J.; Muhler, M. *ChemPhysChem* **2010**, *11*, 2521−2529. (c) Bond, G. C.; Louis, C.; Thompson, D. T. *Catalysis by gold*; Imperial College Press: London, 2006. (d) Widmann, D.; Liu, Y.; Schüth, F.; Behm, R. *J. Catal.* **2010**, *276*, 292−305. (e) Grunwaldt, J. D.; Maciejewski, M.; Becker, O. S.; Fabrizioli, P.; Baiker, A. *J. Catal.* **1999**, *186*, 458−469. (f) Hashmi, A. S. K.; Hutchings, G. J. *Angew. Chem., Int. Ed.* **2006**, *45*, 7896−7936. (g) Haruta, M. *Catal. Today* **1997**, *36*, 153−166.

(2) Widmann, D.; Behm, R. J. *Angew. Chem., Int. Ed.* **2011**, *50*, 10241−10245.

(3) Murdoch, M.; Waterhouse, G. I. N.; Nadeem, M. A.; Metson, J. B.; Keane, M. A.; Howe, R. F.; Llorca, J.; Idriss, H. *Nat. Chem.* **2011**, 489−492.

(4) Primo, A.; Corma, A.; García, H. *Phys. Chem. Chem. Phys.* **2010**, *13*, 886−910.

(5) Gärtner, F.; Losse, S.; Boddien, A.; Pohl, M.-M.; Denurra, S.; Junge, H.; Beller, M. *ChemSusChem* **2012**, *5* (3), 530−533.
(6) Bowker, M.; Millard, L.; Greaves, J.; James, D.; Soares, J. *Gold Bull.* **2004**, *37*, 170−173.
(7) Bowker, M.; Morton, C.; Kennedy, J.; Bahruji, H.; Greves, J.; Jones, W.; Davies, P.; Brookes, C.; Wells, P.; Dimitratos, N. *J. Catal.* **2013**, DOI: 10.1016/j.jcat.2013.04.005.
(8) Du, L.; Furube, A.; Yamamoto, K.; Hara, K.; Katoh, R.; Tachiya, M. *J. Phys. Chem. C* **2009**, *113*, 6454−6462.
(9) Comotti, M.; Li, W.-C.; Spliethoff, B.; Schüth, F. *J. Am. Chem. Soc.* **2006**, *128*, 917−924.
(10) Fuku, K.; Sakano, T.; Kamegawa, T.; Mori, K.; Yamashita, H. *J. Mater. Chem.* **2012**, *22*, 16243−16247.
(11) Mori, K.; Miura, Y.; Shironita, S.; Yamashita, H. *Langmuir* **2009**, *25* (18), 11180−11187.
(12) Tauster, S. J.; Fung, S. C.; Garten, R. L. *J. Am. Chem. Soc.* **1978**, *100*, 170−175.
(13) Dulub, O.; Hebenstreit, W.; Diebold, U. *Phys. Rev. Lett.* **2000**, *84*, 3646−3649.
(14) de La Peña O'Shea, V. A.; Consuelo Álvarez Galván, M.; Platero Prats, A. E.; Campos-Martin, J. M.; Fierro, J. L. G. *Chem. Commun.* **2011**, *47*, 7131−7133.
(15) Arjad, A. B.; Yarmoff, J. A. *J. Phys. Chem. C* **2012**, *116*, 23377−23382.
(16) (a) Liu, J. J. *ChemCatChem* **2011**, *3*, 934−948. (b) Hansen, P. L.; Wagner, J. B.; Helveg, S.; Rostrup-Nielsen, J. R.; Clausen, B. S.; Topsøe, H. *Science* **2002**, *295*, 2053−2055.
(17) Diebold, U. *Surf. Sci. Rep.* **2003**, *48*, 53−229.
(18) Fu, Q.; Wagner, T. *Surf. Sci. Rep.* **2007**, *62*, 431−498.
(19) Freund, H.-J.; Meijer, G.; Scheffler, M.; Schlögl, R.; Wolf, M. *Angew. Chem., Int. Ed.* **2011**, *50*, 10064−10094.
(20) Ohyama, J.; Yamamoto, A.; Teramura, K.; Shishido, T.; Tanaka, T. *ACS Catal.* **2011**, *1*, 187−192.
(21) Gong, X.-Q.; Selloni, A.; Dulub, O.; Jacobson, P.; Diebold, U. *J. Am. Chem. Soc.* **2008**, *130*, 370−381.
(22) (a) Anpo, M.; Thomas, J. M. *Chem. Commun.* **2006**, *31*, 3273. (b) Thomas, J. M.; Raja, R.; Lewis, D. W. *Angew. Chem., Int. Ed.* **2005**, *44*, 6456−6482.
(23) (a) Anpo, M.; Chiba, K. *J. Mol. Catal.* **1992**, *74*, 207−212. (b) Ikeue, K.; Yamashita, H.; Anpo, M.; Takewaki, T. *J. Phys. Chem. B* **2001**, *105*, 8350−8355. (c) Danon, A.; Stair, P. C.; Weitz, E. *Catal. Lett.* **2011**, *141*, 1057−1066. (d) Ulagappan, N.; Frei, H. *J. Phys. Chem. A* **2000**, *104*, 7834−7839. (e) Yang, C.-C.; Vernimmen, J.; Meynen, V.; Cool, P.; Mul, G. *J. Catal.* **2011**, *284*, 1−8.
(24) Mei, B.; Pougin, A.; Muhler, M.; Strunk, J. *J. Catal.* **2013**, *306*, 184−189.
(25) Mei, B. Ph. D. Thesis, Ruhr University Bochum, 2013.
(26) Mei, B.; Becerikli, A.; Pougin, A.; Heeskens, D.; Sinev, I.; Grünert, W.; Muhler, M.; Strunk, J. *J. Phys. Chem. C* **2012**, *116*, 14318−14327.
(27) Anpo, M.; Yamashita, H.; Ichihashi, Y.; Ehara, S. *J. Electroanal. Chem.* **1995**, *396*, 21−26.
(28) Gao, X.; Wachs, I. E. *Catal. Today* **1999**, *51*, 233−254.
(29) Danon, A.; Stair, P. C.; Weitz, E. *Catal. Lett.* **2011**, *141*, 1057−1066.
(30) Busser, G. W.; Mei, B.; Muhler, M. *ChemSusChem* **2012**, *5*, 2200−2206.
(31) Hirakawa, T.; Nosaka, Y. *Langmuir* **2002**, *18*, 3247−3254.
(32) Marschall, R.; Mukherji, A.; Tanksale, A.; Sun, C.; Smith, S. C.; Wang, L.; Lu, G. Q. *J. Mater. Chem.* **2011**, *21*, 8871−8879.
(33) Gao, X.; Bare, S. R.; Fierro, J. L. G.; Banares, M. A.; Wachs, I. E. *J. Phys. Chem. B* **1998**, *102*, 5653−5666.
(34) (a) Fang, X.; Mark, G.; von Sonntag, C. *Ultrason. Sonochem.* **1996**, *3*, 57−63. (b) Liu, G.; Wang, L.; Sun, C.; Yan, X.; Wang, X.; Chen, Z.; Smith, S. C.; Cheng, H.-M.; Lu, G. Q. *Chem. Mater.* **2009**, *21*, 1266−1274.
(35) Buso, D.; Pacifico, J.; Martucci, A.; Mulvaney, P. *Adv. Funct. Mater.* **2007**, *17*, 347−354.
(36) Escamilla-Perea, L.; Nava, R.; Pawelec, B.; Rosmaninho, M.; Peza-Ledesma, C.; Fierro, J. *Appl. Catal., A* **2010**, *381*, 42−53.
(37) (a) Tanaka, A.; Ogino, A.; Iwaki, M.; Hashimoto, K.; Ohnuma, A.; Amano, F.; Ohtani, B.; Kominami, H. *Langmuir* **2012**, *28*, 13105−13111. (b) Kaur, R.; Pal, B. *J. Mol. Catal. A* **2012**, *355*, 39−43.
(38) Müller, M.; Turner, S.; Lebedev, O. I.; Wang, Y.; van Tendeloo, G.; Fischer, R. A. *Eur. J. Inorg. Chem.* **2011**, *12*, 1876−1887.
(39) Zhang, L.; Miller, B. K.; Crozier, P. A. *Nano Lett.* **2013**, *13*, 679−684.
(40) Kelly, L. K.; Coronado, E.; Zhao, L.; Schatz, G. C. *J. Phys. Chem. B* **2003**, *107*, 668−677.